Saudi Journal of Biological Sciences 27 (2020) 3199–3207

Contents lists available at ScienceDirect

Saudi Journal of Biological Sciences

journal homepage: www.sciencedirect.com

Original article

# Synergistic effect of TEMPO-coated $TiO_2$ nanorods for PDT applications in MCF-7 cell line model

M. Fakhar-e-Alam [a,*], Aqrab-ul-Ahmad [b], M. Atif [c], K.S. Alimgeer [d], Muhammad Suleman Rana [e], Nafeesah Yaqub [c], W. Aslam Farooq [c], Hijaz Ahmad [f]

[a] Department of Physics, GC University, 38000 Faisalabad, Pakistan
[b] School of Physics and School of Microelectronics Dalian University of Technology, Dalian 116024, China
[c] Deprtment of Physics and Astronomy, College of Science, King Saud University, Riyadh 11451, Saudi Arabia
[d] Department of Electrical Engineering, COMSATS University, Islamabad, Pakistan
[e] National Institute of Health, Islamabad, Pakistan
[f] Department of Basic Sciences, University of Engineering and Technology, Peshawar 25000, Pakistan

ARTICLE INFO

*Article history:*
Received 14 July 2020
Revised 7 September 2020
Accepted 13 September 2020
Available online 23 September 2020

*Keywords:*
TEMPO
Titanium dioxide nanorods ($TiO_2$ NRs)
Photodynamic therapy (PDT)
MCF-7 cell line

ABSTRACT

This study focuses on the synthesis, characterization, and assessment of the synergistic effect of 2,2,6,6, tetramethylpiperidine-N-oxyl (TEMPO)-coated titanium dioxide nanorods ($TiO_2$ NRs) for photodynamic therapy (PDT). Firstly, $TiO_2$ NRs were synthesized by the sol–gel technique. Then, TEMPO was grafted on $TiO_2$ NRs with the aid of oxoammonium salts. Next, the final product was characterized by applying manifold characterization techniques. X-ray diffraction was used to perform crystallographic analysis; transmission electron microscopy (TEM) was used to conduct morphological analysis; Fourier transform infrared (FTIR) and Raman spectra were recorded to perform molecular fingerprint analysis. Furthermore, experimental and empirical modeling was performed to confirm the suitability of as-prepared samples for PDT applications using (MCF-7 cell line) Human Breast Cancer cell line. Our results revealed that bare $TiO_2$ NRs did not exhibit a significant response for therapeutic applications compared to TEMPO-conjugated $TiO_2$ NRs in the dark; however, they exhibited a prominent response for the PDT application under UV-A light. Therefore, it is concluded that TEMPO-coated $TiO_2$ NRs shows the synergistic response for therapeutic approach under UV-A light irradiation. In addition, TEMPO capped TiO2 nanorods not only overcome the multidrug resistance (MDR) hindrance but also exhibit excellent response for cancer cell (MCF-7 cells) treatment only under UV light irradiation via PDT. It is expected that the proposed $TiO_2$ NRs + TEMPO nanocomposite, which is suitable for PDT treatment, may be essential for photodynamic therapy.


## 1. Introduction

Cancer is abnormal proliferation in the cells of the body, which cannot be easily restricted (Mokwena et al., 2018). Cancers primarily originate from DNA variation, which affects the fabrication of normal cells. Photodynamic therapy is a treatment for cancerous cells that uses photosensitizer (PS) drugs activated by laser light. In the past decades, many researchers have tried to treat cancer using PDT (Mokwena et al., 2018; Vrouenraets et al., 2003; Kashtan et al., 1991). PDT is a less invasive method, which utilizes a very short minimum time spam; PDT shows good results (Kwiatkowski et al., 2018).

Owing to the progress of nanotechnology, there is a need to explore new possible interactions between nanotechnology tools and biological tissues or cells for curing and early detection of various human diseases. Numerous attempts have been made to study the role of different $TiO_2$ nanostructures as anti-cancer and image contrast agents (Yuan and Song, 2018; Mendez and Daniele, 2011). However, there is still a gap in improving their properties for PDT application (Zeng et al., 2013). Furthermore, in recent years, metal-free organic nitroxide radicals-modified nanomaterials (Au, $Fe_2O_3$) have been successfully applied as anti-cancer agents for PDT and as

* Corresponding author.
*E-mail address:* fakhar@gcuf.edu.pk (M. Fakhar-e-Alam).
Peer review under responsibility of King Saud University.

Production and hosting by Elsevier

https://doi.org/10.1016/j.sjbs.2020.09.027
1319-562X/

$T_1$ contrast agents to study the redox condition in cancerous tumors (Xia et al., 2018; Shen et al., 2019). TEMPO is a metal-free organic compound, which has promising applications in medicine (Isogai et al., 2011). Similarly, hybrid nanocomposites of $TiO_2$ nanostructures and polymers can be utilized in biomedical fields (especially in PDT) owing to their unique physical and chemical properties.

In this study, we explored a water-soluble hybrid TEMPO-grafted $TiO_2$ NR nanocomposite for application in PDT. The main purpose of this study was the successful synthesis of TEMPO-labelled $TiO_2$ NRs to improve the efficacy of diagnosis and treatment of cancer cells using PDT. Firstly, the successful growth of $TiO_2$ NRs and TEMPO-coated $TiO_2$ NRs was achieved (see Fig. 1). Secondly, the grown product was confirmed and their toxicity and phototoxic compatibility of the proposed nanocomposite was investigated in an MCF-7 cell line for PDT towards its capability in a human breast cancer cells. Our results showed that TEMPO-capped $TiO_2$ had higher efficacy towards cancer cells. In this article the author experimental strategy was how TEMPO coated TiO2 nanorods are favorable for PDT treatment after overcoming multidrug resistance hinderance towards breast cancer model. In addition, how PDT results were obtained in Tempo coated TiO2 nanordos localized into MCF-7 cells in the dark and under irradiation of UV-A light.

## 2. Materials and methods

### 2.1. Synthesis of titanium dioxide nanorods ($TiO_2$ NRs)

Initially, a solution containing 15 mL of ethanol and 5 mL of distilled water was prepared; then, 3 mL of titanium isopropoxide [$Ti(OC_3H_7)_4$] was added drop wise. The $Ti(OC_3H_7)_4$:$C_2H_5OH$:$H_2O$ molar ratio was set at 1:1. Another solution, containing 1.7 g of oxalic acid in distilled water, was separately prepared (Nian and Teng, 2006). Then, both solutions were mixed under continuous stirring by keeping the pH of the solution at approximately 6. Next, the solution was slowly heated to 75 °C until gel was formed. Then, gel was dehydrated at 125 °C for 2.5 h. To obtain desired $TiO_2$ NRs, the end product was sintered at 450 °C for 4 h (Koo et al., 2006).

### 2.2. Preparation of TEMPO-coated $TiO_2$ nanorods

TEMPO-functionalized $TiO_2$ NRs were synthesized during oxoammonium salts according to previously reported literature (Nieto-López et al., 2013). Herein, to functionalize $TiO_2$ NRs using oxoammonium salts, first, a 100-mL solution of $CH_2Cl_2$ with 4.25 g of triethylamine ($Et_3N$) was added into a glass reactor equipped with a condenser, magnetic stirrer, and $N_2$ gas supply. Then, 2 g of $TiO_2$ NRs was added and vigorously stirred for 15 min. Second, a solution of 10 g of Br-TEMPO in 80 mL of $CH_2Cl_2$ was added drop wise. The reaction was completed in few minutes. However, to confirm successful functionalization, the reaction mixture was stirred for 5 h under nitrogen environment. Finally, TEMPO-functionalized $TiO_2$ NRs were vacuum-filtered and dried in a vacuum oven overnight at room temperature.

### 2.3. Cell culturing

Breast Cancer Cells (MCF-7 Cells) were cultured and maintained at 37 °C in minimum essential media (10) containing 10% fetal bovine serum (FBS), 2 mL of glutamine, nonessential amino acids, and Hank's salt. In addition, the MCF-7 cells were sub-cultured two or three times per week. Then, the cells were harvested by 0.25% trypsin once they reached the confluence of 75–85% (Iqbal et al., 2019a, 2019b).

### 2.4. Cell labeling and PDT treatment

Breast Cancer Cells (MCF-7 Cells) line was sub-cultured in a 96-well plate and was labelled with various concentrations of $TiO_2$ NRs and Tempo coated $TiO_2$ nanorods (i.e., 0–80 μg/mL) and incubated at 37 °C for 24 h with 10% FBS and 5% $CO_2$, as described (Fakhar-e-Alam et al., 2011). The 96-well plates were arranged in 10 columns; each column consisted of 8 wells, 4 wells in each column were labelled with $TiO_2$ nanorods and remaining 4 wells of column were exposed with TEMPO coated with $TiO_2$ nanorods. Absorbance of both samples (TiO2 nanorods, TEMPO Capped with TiO2 nanorods) were tested via microplate reader having filter 490 nm and 510 nm available in microplate reader (Fakhar-e-Alam et al., 2011). First 10 columns were labeled with varying concentrations of a $TiO_2$ nanorod dispersion solution ranging from 0 μg/mL to 80 μg/ml pure and coated with TEMPO, and the last two columns were kept as the standard. The abovementioned cell line was treated with $TiO_2$ NRs with and without the presence of laser light (≈UV-A light), UV lamp having option of UV-A, UV-B and UV-C light wavelength were applied for PDT results and their cellular viability was determined after 24 h of incubation (Fakhar-e-Alam et al., 2014). Author selected the UV-A light having low dose of 20 J/cm$^2$ due to match able absorbance spectrum of $TiO_2$

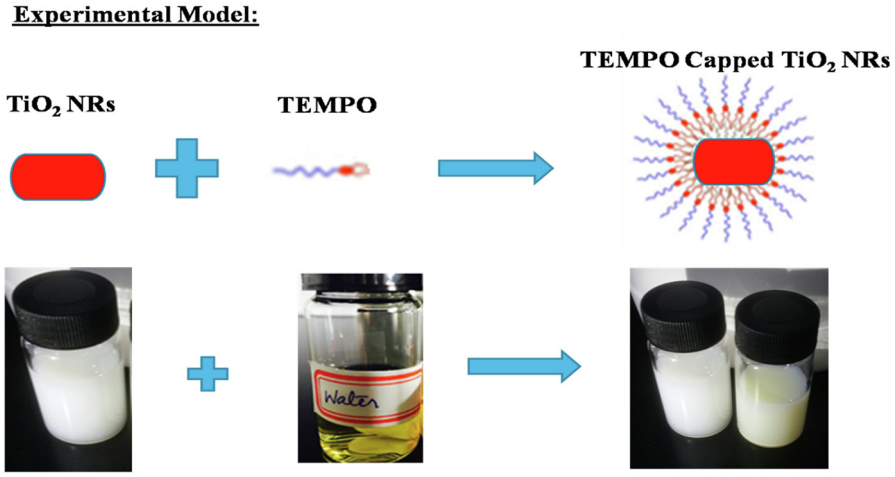


**Fig. 1.** Schematic diagram of the experimental model of TEMPO capping of $TiO_2$ NRs.

nanordos which also exist in the mentioned region, so that countable photochemicals reactions stimulated and significant ROS liberated which leads to cell apoptosis/necrosis. This threshold dose of UV-A light able to produce photochemical reaction but not capable for DNA mutation or direct cell killing phenomena. We cannot select visible part of light region because no TiO2 absorbance peak were recorded in visible region very superficial part of PDT effect were expected.

## 3. Results and discussion

### 3.1. Characterization

After the successful synthesis of $TiO_2$ NRs, their crystal structure was confirmed by X-ray diffraction (XRD). The XRD instrument (Panalytical X' Pert-Pro) was operated at 30-mA current and 40-kV voltage. The scanning range was adjusted from 0° to 90° (2θ) with the step size of ≈0.025°. Structural analysis was performed by transmission electron microscopy (TEM). Fourier transform infrared (FTIR) spectroscopy (Spectrum 2, Perkin Elmer) was used to analyze the chemical composition and bonding of synthesized powder. Raman spectroscopy was used to identify vibrational modes of molecules; the frequency range was 3600–100 $cm^{-1}$, and the resolution was 0.3 $cm^{-1}$. Moreover, absorption spectra of the samples were recorded by a UV–vis spectrophotometer (Model NO. AE-S70-2U, Single beam spectrophotometer with highly stable Optics 4 cell holder, 190–1100 nm, bandwidth 2 nm which is our region of interest) in the wavelength range of 200–700 nm but our region of interest 200–350 nm.

#### 3.1.1. XRD analysis and UV–Visible spectroscopy

The XRD pattern of $TiO_2$ NRs demonstrated the diffraction peaks of anatase and rutile phases at 27.5, 54, 36, and 42°, as shown in Fig. 2. It is observed that after the growth of $TiO_2$ NRs, the anatase phase peak intensities were higher than those of the rutile phase, which indicated that during growth, anatase phase was dominant rather than rutile phase. All peaks were in good agreement with the standard spectrum (JCPDS no.: 88-1175 and 84-1286) and previous published data (Nian and Teng, 2006). The average crystallite size of nanoparticles was estimated by Scherer's formula:

$$D_\beta = 0.89\lambda/\beta\cos\theta$$

The crystallite size of synthesized rods was 36.13 ± 16.06 for plane (101) and 55.12 ± 25.30 for plane (211). It was observed that the crystallite size increased when the diffraction peak intensities decreased.

The UV measurements of synthesized samples, shown in Fig. 2 (b), were studied to inspect the absorption behavior. It is observed that the spectrum of $TiO_2$ has a very sharp edge from 300 nm to 400 nm, which indicates that $TiO_2$ NRs absorb light primarily in the ultraviolet region (Rao et al., 2014). The spectrum of TEMPO has an edge between 250 nm and 300 nm. Furthermore, light absorption decreases for TEMPO-capped $TiO_2$ NRs ($TiO_2$ + TEMPO).

#### 3.1.2. TEM measurements

The morphological and structural analysis of bare $TiO_2$ nanorods and TEMPO-coated $TiO_2$ NRs was performed using TEM. The samples were prepared by making a uniform dispersion of TEMPO-coated $TiO_2$ NRs in isopropyl alcohol and putting it onto a TEM grid coated with a thin film of amorphous carbon (Miao et al., 2004). Fig. 3(a) shows the TEM image of bare $TiO_2$ nanorods, which reveals that nanorods have an average length of approximately 350 nm and a diameter of approximately 20 nm. Fig. 3 (b)–(d) showed the images of TEMPO-coated $TiO_2$ NRs at different magnifications. It is observed that after TEMPO capping, agglomeration occurs between nanorods. This may be due to the organic nature of TEMPO. Fig. 3(d) clearly shows that during the growth of nanorods, the shape of nanorods at the end is nearly round.

#### 3.1.3. FTIR analysis

The bonding nature of individual $TiO_2$ NRs, TEMPO, and TEMPO-capped $TiO_2$ NRs was confirmed by FTIR spectra, as shown in Fig. 4 (a)–(c). Fig. 4(a) shows that a strong absorption peak of the stretching mode of $TiO_2$ is at approximately 1162 $cm^{-1}$, while the peak shifts to 1639 $cm^{-1}$ in the presence of other functional group, H—O—H, owing to physically absorbed moisture on the sample. Moreover, the presence of the O—H stretching mode is also observed at 3400 $cm^{-1}$. Fig. 4(b) shows the spectra of individual TEMPO. The two shoulder peaks at 973 $cm^{-1}$ and 1467 $cm^{-1}$ are due to the presence of C—N bonds in TEMPO. However, the peaks attributed to the presence of $CH_3$ absorption shifted from 2929 $cm^{-1}$ to 2931 $cm^{-1}$. Fig. 4(c) shows TEMPO-capped $TiO_2$ NRs and all major stretching peaks related to $TiO_2$ NRs and TEMPO, are described in the abovementioned discussion of individual sam-

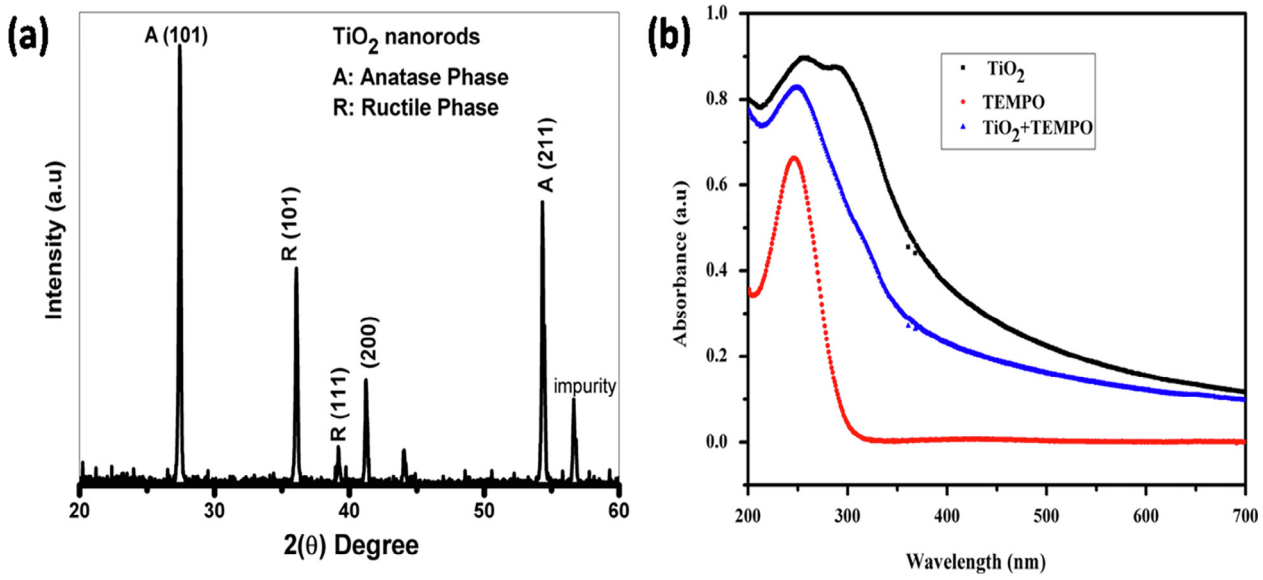


**Fig. 2.** (a) XRD pattern of $TiO_2$ NRs and (b) UV–vis spectra of $TiO_2$ NRs, TEMPO, and TEMPO + $TiO_2$ NRs.

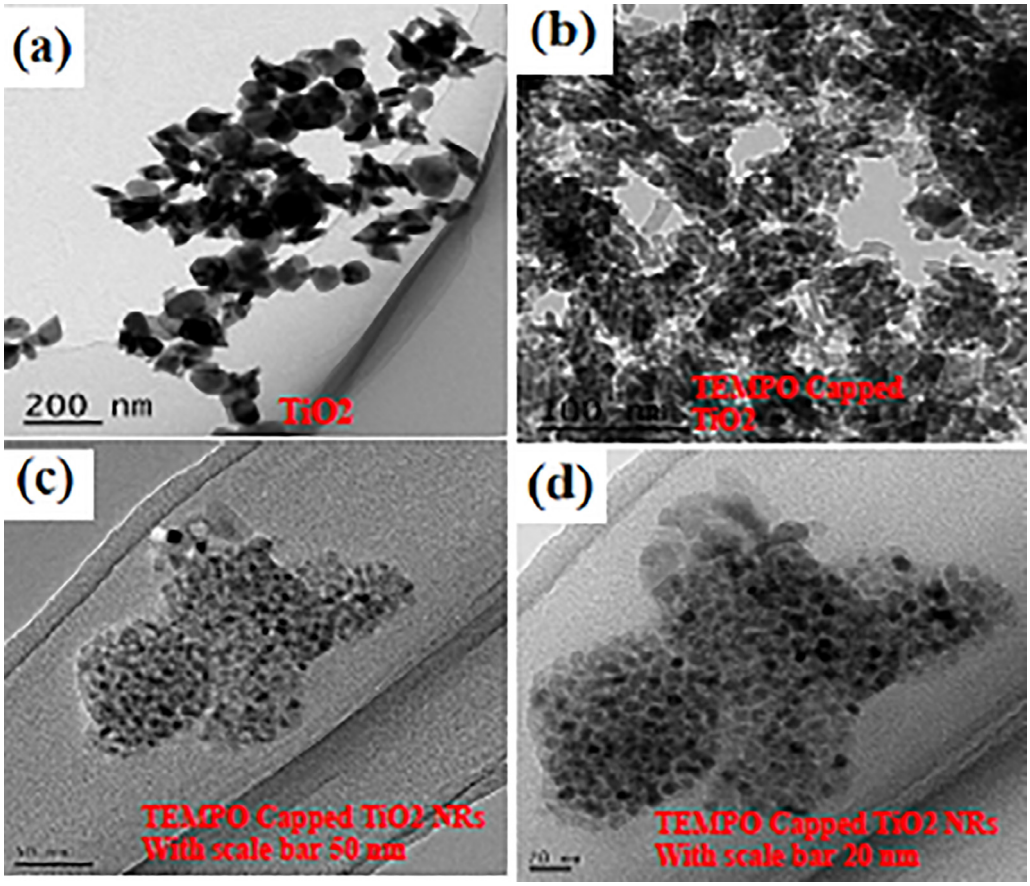


**Fig. 3.** TEM images of bare $TiO_2$ NRs and TEMPO-caped $TiO_2$ NRs at different magnifications.

ples. Consequently, FTIR spectra confirms the results in previous reports on TEMPO-capped $TiO_2$ NRs (Nieto-López et al., 2013).

### 3.1.4. Raman measurements

Using Raman spectroscopy, we can identify vibration modes of molecular bonds in synthesized samples. This technique provides accurate measurement of the percentage of exposed facets from the perspective of molecular bonding with fewer measurement errors. Therefore, Raman spectroscopy allows us to quantitatively measure the percentage of facets in $TiO_2$, TEMPO, and TEMPO-coated $TiO_2$, as shown in Fig. 5. Fig. 5(a) shows that the major phase of $TiO_2$ NRs is anatase, which is consistent with the XRD data. Fig. 5(b) shows the different stretching vibration modes of molecular bonds such as C—C, C—H, and alkyl chain in pristine TEMPO. Fig. 5(c) shows the combined spectra of TEMPO and $TiO_2$ NRs with stronger bands of $TiO_2$ and weaker shoulders at approximately 1439 $cm^{-1}$ and 2916 $cm^{-1}$ (attributed to TEMPO) (Zhang et al., 2012).

### 3.1.5. MTT Assay/Analysis:

The cytotoxic effects of TEMPO, $TiO_2$ NRs, and TEMPO with $TiO_2$ NRs were investigated in MCF-7 (breast cancer) cells. Fig. 6(a) and (b) clearly show that the mentioned form of working solution does not have considerable toxicity difference in the abovementioned breast cancer cell model when they are exposed to TEMPO, $TiO_2$ NRs, and TEMPO-coated $TiO_2$ NRs. Loss in MCF-7 cell viability (but not significant) was recorded after the exposure of MCF-7 cells to 0–500 μg/mL of TEMPO, $TiO_2$ NRs, and TEMPO-labeled $TiO_2$ NRs. Only 20% loss in MCF-7 cells was observed when the chosen working solution dose of TEMPO-coated $TiO_2$ NRs was used. The same experiment was conducted to evaluate the anticancer activity of nanoparticles towards Hela and MCF-7 cell models (Fakhar-e-Alam et al., 2012b; ul Rehman et al., 2017; ul Rehman et al., 2020). In addition, the empirical modeling results match the experimentally recorded results, which is in good agreement with previously published data.

Fig. 6 (b) shows the mathematical model, which uses two exponential functions. The values of respective unknown variables are extracted using the least squares error method. The results are shown in Table 1.

$$M_i = A_i e^{a_i} + B_i e^{b_i} \quad (1)$$

where i = 1, 2, 3; $M_i$ represents the model; $A_i$, $a_i$, $B_i$, and $b_i$ are unknown constants to be evaluated using the least squares error method.

### 3.1.6. PDT treatment of MCF-7 cells

Fig. 7(a) and (b) show three sample of $TiO_2$ + TEMPO at three different exposures of light. The first sample was evaluated in the dark; the analysis showed that cell viability was not affected; thus, in the dark, cell lining was not ruptured. The second sample was exposed to UV light; then, the viability of cell was decreased but not considerably. The last sample was exposed to PDT for 10 min and showed the maximum damage of cancer cell lining. This means that PDT absorption considerably affected cell lining. These results closely supports the previous published results (Bavanilatha et al., 2019). Similar data were also obtained for in vitro and in vivo studies (Fakhar-e-Alam et al., 2012a). Specifically, significant loss in cell viability has been recorded and reported. Fig. 7(c) and (d) show the results for four samples of

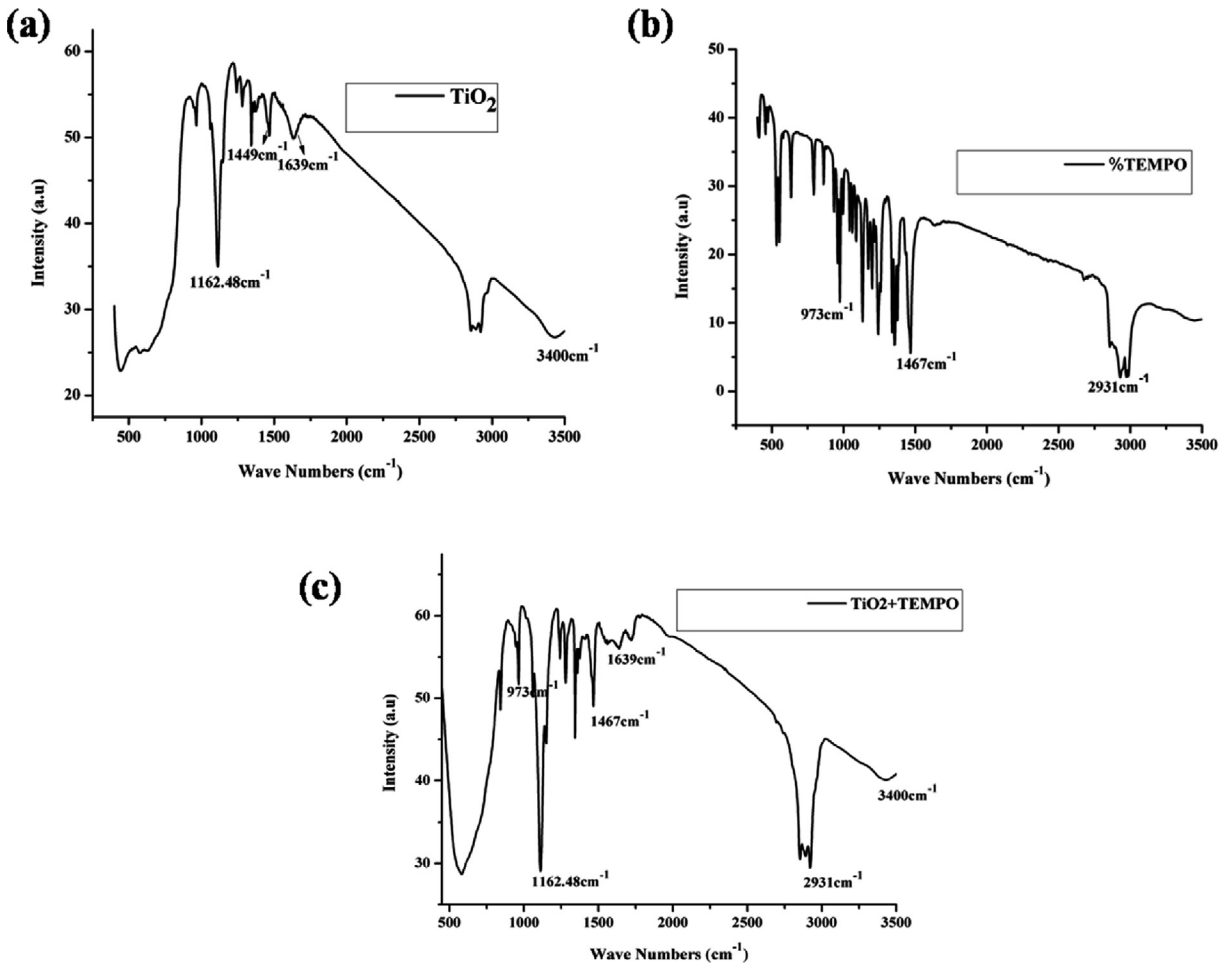


**Fig. 4.** (a–c) FTIR spectra of individual $TiO_2$ NRs, pristine TEMPO, and $TiO_2$ + TEMPO, respectively.

$TiO_2$ + TEMPO-treated cells that were treated for different periods of time and exposed to UV light. The first sample contained cells that were treated in the dark; there was either no effect or low effect on cancer lining. The second sample contained cells that were exposed to UV light for 5 min; for this sample, cell viability decreased but the effect was not significant. For the third sample, exposure time was increased to 10 min, and the effect increased as in the fourth sample. These results showed that with an increase in the UV exposure time, the cell viability decreased. The results of this research are in good agreement with the previous published data (Lu et al., 2015). Toxicity occurs because there is an excess of low density lipoprotein (LPL) receptors in liver cancer tissue, which attracts more antioxidant agents occupied by TEMPO-treated $TiO_2$ NRs. This interaction produces many chemical reactions, which lead to the production of reactive oxygen species (ROS) and loss of mitochondrial membrane and initiates the carcinogenic killing mechanism. However, in the absence of suitable light, there is less damage owing to the presence of normal quantity of low density lipoprotein (LDL), high density lipoprotein (HDL), and very high density lipoprotein (VHDL) receptors.

Moreover, it was determined that cell viability loss for MCF-7 cells was approximately 80% when using an effective UV-A light dose of 10 J/cm$^2$; the calculated loss for the dark portion of TEMPO with $TiO_2$ NRs was only approximately 20%. This result implies that TEMPO with $TiO_2$ under UV-A illumination is useful for breast cancer treatment applications which is in good agreement with previously published data (Rehana et al., 2017).

Similarly, the data analysis shown in Fig. 7(b) and (d) was performed in the same way using Eq. (1) with different coefficients. It is important to note that the modeled curve matched well the presented experimental data.

### 3.1.7. Comparison graph

Fig. 8(a) and (b) shows six 96-well plates containing MCF-7 cells. The cells were cultured and assigned to five groups with different chemical ligands/concentration to control MCF-7: TEMPO toxicity assessment towards MCF-7 cells, $TiO_2$ NRs toxicity assessment towards MCF-7 cells, TEMPO with $TiO_2$ toxicity assessment towards MCF-7 cells, only UV light toxicity assessment towards MCF-7 cells, and PDT treatment (labeling of TEMPO + $TiO_2$ with MCF-7 cells under suitable UV light exposure) of MCF-7 cells. The most significant results for breast cancer treatment analysis in terms of PDT treatment were recorded (approximately 80% cell viability loss for PDT treatment of MCF-7 cells). The results were tested three times for every group in the experimental arrangement. Fig. 8(a) and (b) shows surface fitting for the data. The following polynomial is selected as candidate function to model the data.

$$\%Cell\,viability = p00 + p10x + p01y + p20x^2 + p11xy + p02y^2 + p30x^3 + p21xy^2 + p12yx^2 + p03y^3$$

Percent cell viability is a 3D function that depends on x (i.e., different models) and y (i.e., different concentration levels). The vertical axis in the graph shows % cell viability. The unknown

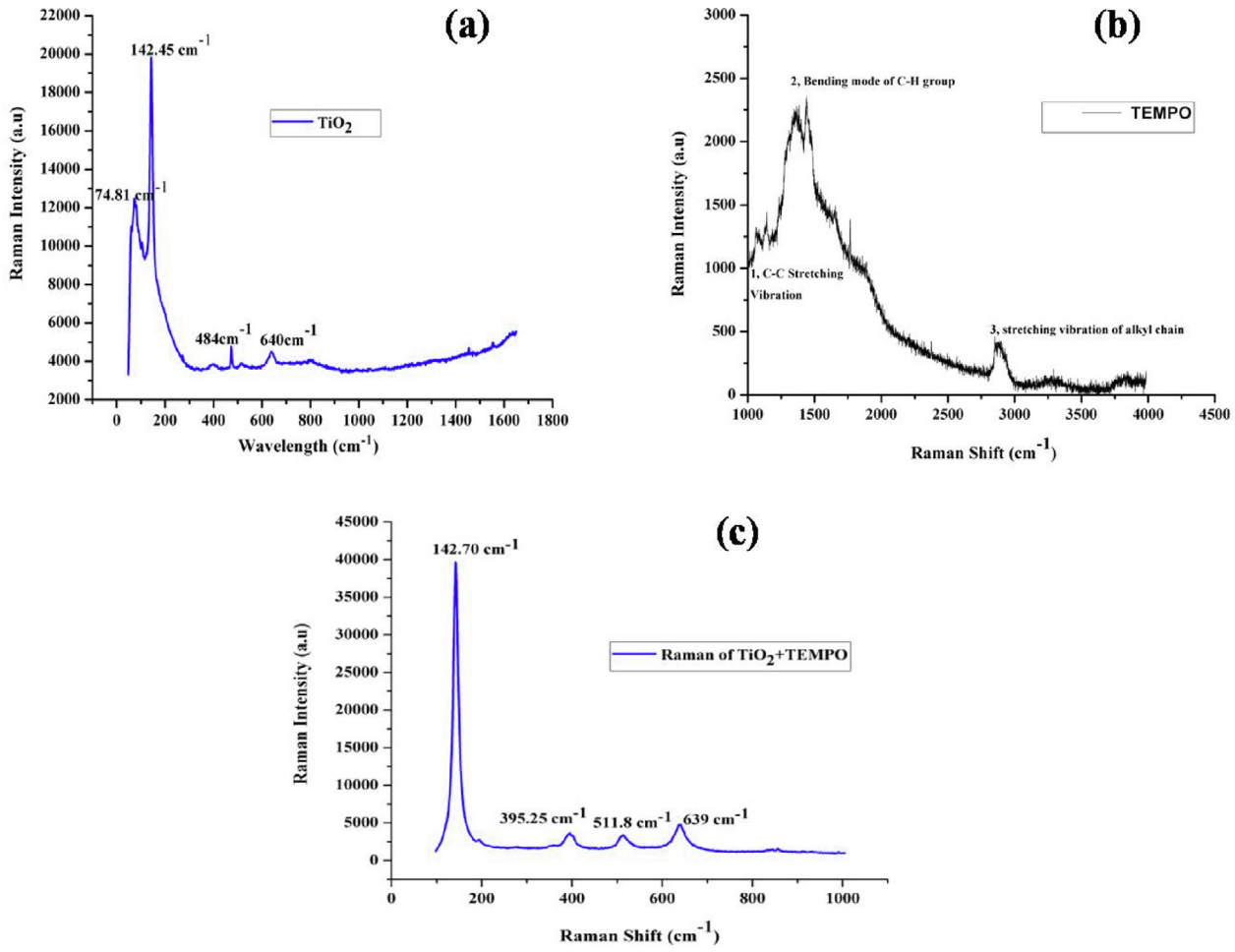


**Fig. 5.** (a–c) Raman spectra of $TiO_2$ NRs, TEMPO, and TEMPO + $TiO_2$, respectively.

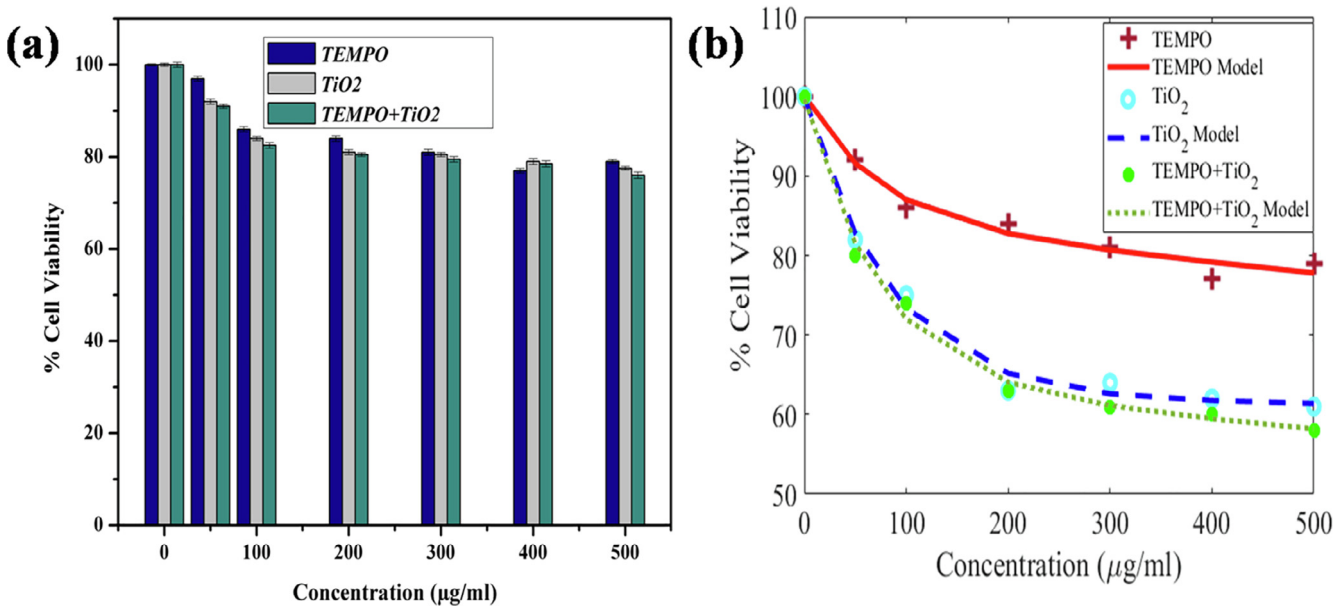


**Fig. 6.** Percent loss in MCF-7 cell viability. (a) Experimental data. (b) Experimental data vs. empirical modulated data.

coefficients are extracted through the surface fitting technique and are listed in table 2. It is noted that the control model has less variation in % cell viability with an increase in concentration (µg/mL). TEMPO has a slightly higher variation in % cell viability with an increase in concentration (µg/mL) compared to the control model. $TiO_2$ NRs has a slightly higher variation in % cell viability with an

**Table 1**
Values of unknown parameters in Eq. (1)) are extracted from Fig. 6b) using the least squares error method.

| | *Ai* | *ai* | *Bi* | *bi* | SSE | R-square | Adjusted R-Square | RMSE |
|---|---|---|---|---|---|---|---|---|
| M1 | 15.45 | −0.01398 | 84.6 | −1.678e−04 | 8.982 | 0.977 | 0.9539 | 1.73 |
| M2 | 38.01 | −0.0119 | 61.89 | −1.891e−05 | 10.3 | 0.9918 | 0.9836 | 1.853 |
| M3 | 35.36 | −0.01373 | 64.33 | −2.022e−04 | 7.709 | 0.9944 | 0.9889 | 1.603 |

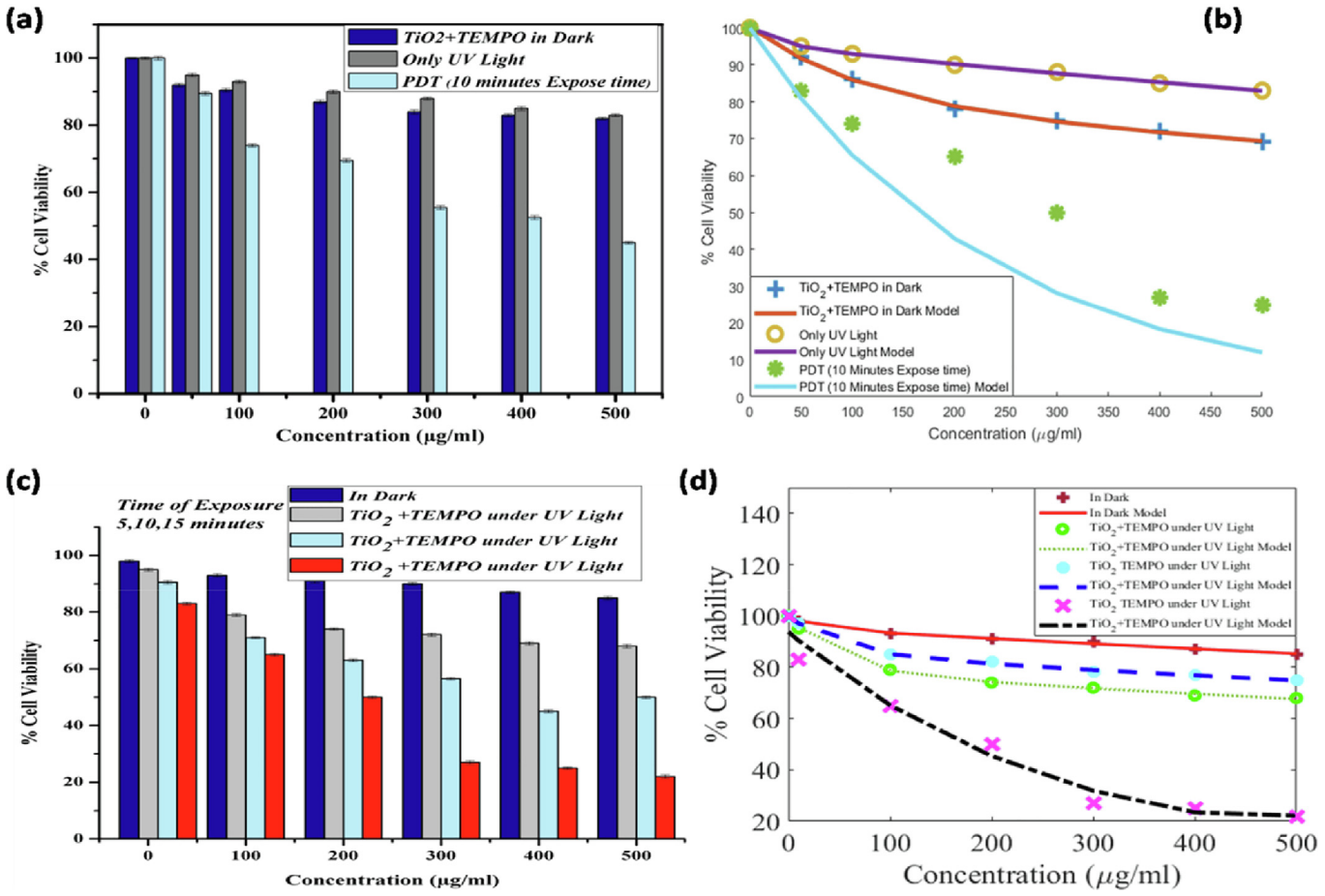


**Fig. 7.** (a–d): Experimental and empirical modeling plots for PDT treatment with $TiO_2$ + TEMPO in the dark and under UV light with different exposure time.

increase in concentration (µg/mL) compared to TEMPO. Similarly, TEMPO + $TiO_2$ NRs shows higher variation. Finally, PDT shows the highest variation in % cell viability with an increase in concentration (µg/mL) compared to any other model.

## 4. Conclusion

In summary, we successfully synthesized a TEMPO-coated $TiO_2$ nanorods, which may be used as an anticancer agent for PDT treatment. By manifold characterization techniques, it was confirmed that TEMPO coated $TiO_2$ nanorods were successfully grown and their morphology, crystallography and molecular finger print were confirmed by applying TEM, XRD and FTIR respectively. The PDT results for the proposed $TiO_2$ NRs + TEMPO nanocomposite showed an approximately 80% and 20% cell viability loss for MCF-7 cells under UV-A (340 nm of light wavelength) with a light dose of 20 J/cm$^2$ and in the dark, respectively. Consequently, it is anticipated that the TEMPO-coated $TiO_2$ NRs synthesis approach under illumination of suitable dose of UV-A light is suitable for the clinical trials for the simultaneous PDT-based cancer cell treatment with high accuracy and sensitivity. It is concluded that TEMPO capped $TiO_2$ nanorods under exposure of UV-A light towards breast cancer model indicate the synergist response of photodynamic effect, which is quite satisfactory for demonstrating the comprehensive treatment plan for breast cancer patients.

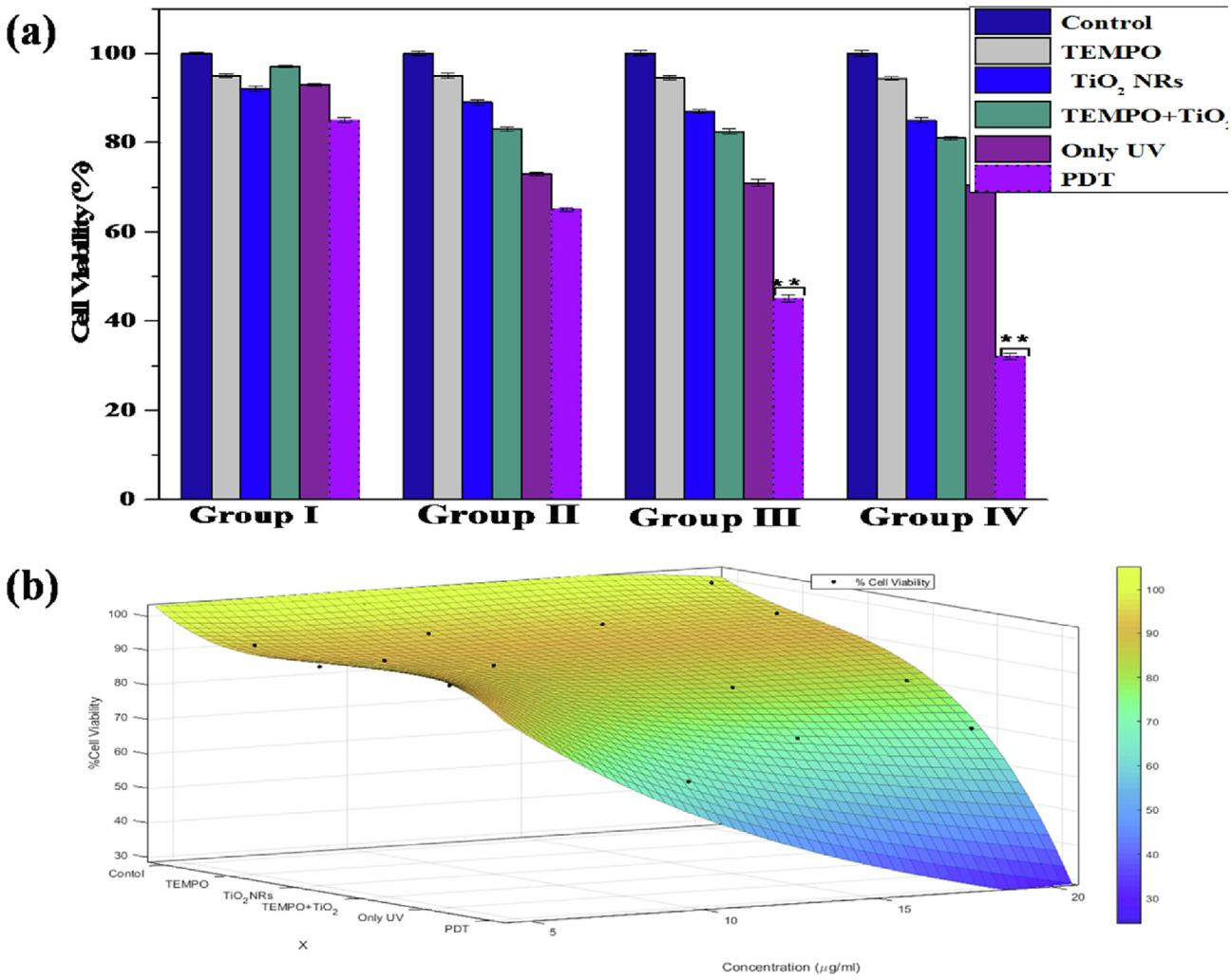


**Fig. 8.** (a–b) shows comparison graph between experimental and modeling.

**Table 2**
values of unknowns in Eq. (1)) are extracted through surface fitting along with parameters of quality goodness.

| Variables | *p00* | *p10* | *p01* | *p20* | *p11* |
|---|---|---|---|---|---|
| Values | *125.9* | −26.25 | −1.887 | *8.845* | −0.05034 |
| Variables | *p02* | *p30* | *p21* | *p12* | *p03* |
| Values | 0.162 | −0.7574 | −0.1919 | 0.03009 | −0.005356 |
| Variables | SSE | R-square | Adjusted R-Square | RMSE | |
| Values | 135.2 | 0.9804 | 0.9678 | 3.108 | |

## Acknowledgments

The authors extend their appreciation to the Higher Education Commission Pakistan under NRPU Project Grant# 8056/Punjab/NRPU/R&D/HEC/2017. The authors extend their appreciation to the Deanship of Scientific Research at King Saud University for funding this work through research group no (RGP-293).

## References

Bavanilatha, M., Yoshitha, L., Nivedhitha, S., Sahithya, S., 2019. Bioactive studies of TiO2 nanoparticles synthesized using Glycyrrhiza glabra. Biocatal. Agric. Biotechnol. 19, 101131.

Fakhar-e-Alam, M., Firdous, S., Atif, M., Khan, Y., Zaidi, S., Suleman, R., Rehman, A., Khan, R., Nawaz, M., Ikram, M., 2011. The potential applications of ZnO nanoparticles conjugated with ALA and photofrin as a biomarker in HepG2 cells. Laser Phys. 21, 2156–2164.

Fakhar-e-Alam, M., Kishwar, S., Siddique, M., Atif, M., Nur, O., Willander, M., 2012. The photodynamic effect of ZnO nanorods and their ligands with different photosensitizers. Rev. Nanoscience Nanotechnol. 1, 40–51.

Fakhar-e-Alam, M., Ali, S.M., Ibupoto, Z.H., Kimleang, K., Atif, M., Kashif, M., Loong, F. K., Hashim, U., Willander, M., 2012. Sensitivity of A-549 human lung cancer cells to nanoporous zinc oxide conjugated with Photofrin. Lasers Med Sci 27, 607–614.

Fakhar-e-Alam, M., Abbas, N., Imran, M., Atif, M., 2014. Apoptotic effect of TiO2 in HepG2 cellular model. J. Optoelectron. Adv. Mater 16, 1481–1486.

Iqbal, S., Fakhar-e-Alam, M., Atif, M., Amin, N., Alimgeer, K., Ali, A., Hanif, A., Farooq, W.A., 2019. Structural, morphological, antimicrobial, and in vitro photodynamic therapeutic assessments of novel Zn+ 2-substituted cobalt ferrite nanoparticles. Results Phys. 15, 102529.

Iqbal, S., Fakhar-e-Alam, M., Atif, M., Ahmed, N., Amin, N., Hanif, A., Farooq, W.A., 2019. Empirical modeling of Zn/Zno nanoparticles decorated/conjugated with fotolon (chlorine e6) based photodynamic therapy towards liver cancer treatment. Micromachines 10, 60.

Isogai, A., Saito, T., Fukuzumi, H., 2011. TEMPO-oxidized cellulose nanofibers. Nanoscale 3, 71–85.

Kashtan, H., Papa, M.Z., Wilson, B.C., Deutch, A.A., Stern, H.S., 1991. Use of photodynamic therapy in the palliation of massive advanced rectal cancer. Dis. Colon Rectum 34, 600–605.

Koo, B., Park, J., Kim, Y., Choi, S.-H., Sung, Y.-E., Hyeon, T., 2006. Simultaneous phase- and size-controlled synthesis of TiO2 nanorods via non-hydrolytic sol– gel reaction of syringe pump delivered precursors. J. Phys. Chem. B 110, 24318–24323.

Kwiatkowski, S., Knap, B., Przystupski, D., Saczko, J., Kędzierska, E., Knap-Czop, K., Kotlińska, J., Michel, O., Kotowski, K., Kulbacka, J., 2018. Photodynamic therapy–mechanisms, photosensitizers and combinations. Biomed. Pharmacother. 106, 1098–1107.

Lu, K., He, Q., Chen, L., Ai, B., Xiong, J., 2015. The comparative PDT experiment of the inactivation of HL60 on modified TiO2 nanoparticles. J. Nanomater. 2015.

Mendez, V., Daniele, S., 2011. New synthesis approach for hybrid Gd (III)–loaded nanocrystalline TiO2 as potential magnetic resonance imaging contrast agents. J. Nanosci. Nanotechnol. 11, 9237–9243.

Miao, L., Tanemura, S., Toh, S., Kaneko, K., Tanemura, M., 2004. Heating-sol–gel template process for the growth of TiO2 nanorods with rutile and anatase structure. Appl. Surf. Sci. 238, 175–179.

Mokwena, M.G., Kruger, C.A., Ivan, M.-T., Heidi, A., 2018. A review of nanoparticle photosensitizer drug delivery uptake systems for photodynamic treatment of lung cancer. Photodiagn. Photodyn. Ther. 22, 147–154.

Nian, J.-N., Teng, H., 2006. Hydrothermal synthesis of single-crystalline anatase TiO2 nanorods with nanotubes as the precursor. J. Phys. Chem. B 110, 4193–4198.

Nieto-López, I., Sanchez-Vazquez, M., Bonilla-Cruz, J., 2013. TiO2-g-TEMPO. A Theoretical and Experimental Study, Macromolecular Symposia, Wiley Online Library, pp. 132–140.

Rao, K.G., Ashok, C., Rao, K.V., Chakra, C.S., Rajendar, V., 2014. Green Synthesis of TiO2 Nanoparticles Using Hibiscus Flower Extract. Conference ICEMS.

Rehana, D., Mahendiran, D., Kumar, R.S., Rahiman, A.K., 2017. Evaluation of antioxidant and anticancer activity of copper oxide nanoparticles synthesized using medicinally important plant extracts. Biomed. Pharmacother. 89, 1067–1077.

Shen, X., Cao, S., Zhang, Q., Zhang, J., Wang, J., Ye, Z., 2019. Amphiphilic TEMPO-functionalized block copolymers: synthesis, self-assembly and redox-responsive disassembly behavior, and potential application in triggered drug delivery. ACS Appl. Polym. Mater. 1, 2282–2290.

ul Rehman, A., Anwer, A.G., Goldys, E.M., 2017. Programmable LED-based integrating sphere light source for wide-field fluorescence microscopy. Photodiagn. Photodyn. Ther. 20, 201–206.

ul Rehman, A., Ahmad, I., Qureshi, S.A., 2020. Biomedical Applications of Integrating Sphere: A Review. Photodiagn. Photodyn. Ther. 101712

Vrouenraets, M.B., Visser, G., Snow, G.B., 2003. Basic principles, applications in oncology and improved selectivity of photodynamic therapy. Anticancer Res. 23, 505–522.

Xia, L., Zhang, C., Li, M., Wang, K., Wang, Y., Xu, P., Hu, Y., 2018. Nitroxide-radicals–modified gold nanorods for in vivo CT/MRI-guided photothermal cancer therapy. Int. J. Nanomed. 13, 7123.

Yuan, P., Song, D., 2018. MRI tracing non-invasive TiO2-based nanoparticles activated by ultrasound for multi-mechanism therapy of prostatic cancer. Nanotechnology 29, 125101.

Zeng, L., Ren, W., Xiang, L., Zheng, J., Chen, B., Wu, A., 2013. Multifunctional Fe3O4–TiO2 nanocomposites for magnetic resonance imaging and potential photodynamic therapy. Nanoscale 5, 2107–2113.

Zhang, K., Fischer, S., Geissler, A., Brendler, E., 2012. Analysis of carboxylate groups in oxidized never-dried cellulose II catalyzed by TEMPO and 4-acetamide-TEMPO. Carbohydr. Polym. 87, 894–900.